The Role of the Central Atom in Structure and Reactivity of Polyoxometalates with Adjacent d-Electron Metal Sites. Computational and Experimental Studies of γ-$[(X^{n+}O_4)Ru^{III}_2(OH)_2(M_{FM})_{10}O_{32}]^{(8-n)-}$ for M_{FM} = Mo and W, and X = Al^{III}, Si^{IV}, P^{V}, and S^{VI}

David Quiñonero, Yan Wang, Keiji Morokuma, Lyuba A. Khavrutskii, Bogdan Botar, Yurii V. Geletii, Craig L. Hill,* and Djamaladdin G. Musaev*

Cherry L. Emerson Center for Scientific Computation and Department of Chemistry, Emory University, 1515 Dickey Drive, Atlanta, Georgia 30322

Received: August 22, 2005; In Final Form: October 4, 2005

The role of the central atom X in the structure and reactivity of di-Ru-substituted γ-Keggin polyoxometalates (POMs), γ-$[(X^{n+}O_4)Ru^{III}_2(OH)_2(M_{FM})_{10}O_{32}]^{(8-n)-}$, where M_{FM} = Mo and W, and X = Al^{III}, Si^{IV}, P^{V}, and S^{VI}, was computationally investigated. It was shown that for both M_{FM} = Mo and W the nature of X is crucial in determining the lower lying electronic states of the polyoxoanions, which in turn likely significantly impacts their reactivity. For the electropositive X = Al^{III}, the ground state is a low-spin state, while for the more electronegative X = S^{VI} the ground state is a high-spin state. In other words, the heteroatom X can be an "internal switch" for defining the ground electronic states of the γ-M_2-Keggin POMs. The obtained trends, in general, are less pronounced for M_{FM} = Mo than for W. On the basis of the comparison of the calculated energy gaps between low-spin and high-spin states of polytungstates and polymolybdates, we predict that the γ-M_2-Keggin polytungstates could be more reactive than their polymolybdate analogues. For purposes of experimental verification the computationally predicted and evaluated polytungstate γ-$[(SiO_4)Ru^{III}_2(OH)_2(OH_2)_2W_{10}O_{32}]^{4-}$ was prepared and characterized.

I. Introduction

The stability and versatility of polyoxometalates (or "POMs"), as well as tunability of their size, charge, composition, and redox properties, make them attractive for applications in catalysis and other technologies.[1] Among many different types of POMs, Keggin-type heteropolyanions, $[(X^{n+}O_4)(M_{FM})_{12}O_{36}]^{(8-n)-}$, where M_{FM}, the metal framework atoms = W and Mo, have attracted considerable attention.[2] Recently, di-d-electron transition-metal-substituted γ-Keggin polytungstates (γ-$[(X^{n+}O_4)M_2(OH)_2W_{10}O_{32}]^{(8-n)-}$ or γ-M_2-Keggin complexes)[3] were reported[4] to catalyze selective oxidations of alkenes, alkanes, and other organic substrates by O_2 and/or H_2O_2. Elucidating the mechanisms of these processes is of central importance for both understanding these complex redox processes and being positioned to optimize catalysts for them. In the larger context, understanding the fundamental properties of POM catalysts capable of such transformations, including the roles of the transition metal centers M, framework metal atoms M_{FM}, heteroatom X, and counterions in POM stability and reactivity, is important.

In this paper we report computational studies of electronic and geometrical structures of the di-Ru^{III}-substituted γ-Keggin POMs (γ-$[(X^{n+}O_4)Ru^{III}_2(OH)_2(M_{FM})_{10}O_{32}]^{(8-n)-}$ or γ-Ru_2-Keggin) for different framework metal atoms (M_{FM} = W and Mo) and heteroatoms (X = Al^{III}, Si^{IV}, P^{V}, and S^{VI}). We analyze the roles of X and M_{FM} in the defining of the lower lying electronic states, geometries and, if possible, the reactivity of these species. We also report the synthesis and characterization of γ-$[(SiO_4)Ru^{III}_2(OH)_2(OH_2)_2W_{10}O_{32}]^{4-}$, one of the computationally evaluated compounds.

* Corresponding authors. E-mail: dmusaev@emory.edu and chill@emory.edu.

II. Computational and Experimental Procedures

A. Computational Details. In these calculations we used the hybrid density functional B3LYP method, which combines the three-parameter exchange functional of Becke (B3)[5] with the Lee−Yang−Parr's (LYP) correlation functional,[6] and the Lanl2dz basis set[7] augmented with the polarization d-function on the X atom (this basis set will be referred to as Lanl2dz + d(X)). Previously, we demonstrated that the B3LYP hybrid density functional method with double-ζ quality basis sets Lanl2dz + polarization d-function on X adequately describes the chemical and physical properties of these compounds.[8] Geometries of all structures were optimized with the analytical gradient method without symmetry constraints. All calculations were performed with the Gaussian03 quantum chemical program package.[9]

B. General Experimental Methods. Electronic spectra were recorded on a Hewlett-Packard 8452A diode array spectrophotometer as acetonitrile solutions, using a 1.000-cm-optical-path quartz cuvette. ^{29}Si NMR measurements were made with a Varian UNITY spectrometer at 79.456 MHz; chemical shifts are reported relative to a 3.6 M $CDCl_3$ solution of tetramethylsilane. Infrared spectra (2% sample in KBr) were recorded on a Nicolet 510 FT-IR spectrometer. The average magnetic susceptibilities were measured on a Johnson Matthey MSB-1 magnetic susceptibility balance as a neat powder at 25 °C. The balance was calibrated by using $Hg[Co(SCN)_4]$ as a standard. Elemental analyses for C, H, and N were performed by Atlantic Microlab (Atlanta, GA) and elemental analyses for Ru, Si, and W were performed by Desert Analytics Laboratory (Tucson, AZ).

C. Synthesis and Characterization of $[(n\text{-}C_4H_9)_4N]_4[\gamma$-$(SiO_4)Ru^{III}_2(OH)_2(OH_2)_2W_{10}O_{32}]\cdot 2H_2O$. Reaction of $K_8[\gamma$-$SiW_{10}O_{36}]\cdot 12H_2O$ with 2 equiv of $RuCl_3\cdot H_2O$ in H_2O (pH 3) produced a brown solution through which O_2 was bubbled for

10.1021/jp054728j CCC: $33.50 © 2006 American Chemical Society
Published on Web 12/10/2005

TABLE 1: Important Calculated Bond Distances (in Å) and Relative Energies (in kcal/mol) of Low-Lying Electronic States of the γ-$[(X^nO_4)Ru_2(OH)_2W_{10}O_{32}]^{(8-n)-}$ for X = Al^{III}, Si^{IV}, P^V, and S^{VI} in C_{2v} Symmetry

	X = Al^{III}			X = Si^{IV}			X = P^V			X = S^{VI}		
bonds	$^1A_1$	$^3B_1$	$^7B_1$	$^1A_1$	$^3B_1$	$^7B_1$	$^1A_1$	$^3B_1$	$^7B_1$	$^1A_1$	$^3B_1$	$^7B_1$
Ru−Ru	2.618	3.062	3.067	2.599	3.028	3.025	2.598	3.022	3.014	2.602	3.019	3.067
$Ru^1-O_b{}^1$	2.083	2.103	2.119	2.077	2.097	2.112	2.073	2.096	2.105	2.070	2.095	2.091
$Ru^1-O_X{}^1$	2.050	2.061	2.364	2.072	2.085	2.446	2.086	2.103	2.560	2.108	2.183	2.933
$Ru^1-O_W{}^1$	2.004	1.996	1.957	1.994	1.986	1.946	1.989	1.980	1.939	1.986	1.973	1.918
$X-O_X{}^1$	1.785	1.798	1.772	1.656	1.662	1.640	1.583	1.584	1.562	1.539	1.535	1.499
$X-O_X{}^3$	1.755	1.765	1.774	1.623	1.630	1.645	1.545	1.550	1.570	1.494	1.503	1.525
$W^1-O_W{}^1$	1.885	1.892	1.929	1.880	1.885	1.920	1.880	1.884	1.919	1.883	1.890	1.929
$W^1-O_X{}^1$	2.360	2.376	2.283	2.465	2.489	2.386	2.539	2.569	2.614	2.510	2.477	2.553
$W^5-O_X{}^3$	2.284	2.266	2.279	2.371	2.339	2.377	2.441	2.404	2.462	2.510	2.477	2.553
$W^7-O_W{}^7$	1.946	1.942	1.946	1.937	1.933	1.938	1.933	1.930	1.936	1.933	1.930	1.940
ΔE	0.0	1.6	10.9	0.0	2.7	1.8	0.0	−1.1	−10.9	0.0	−2.2	−36.1

30 min. Addition of 5 equiv of $(n\text{-Bu})_4NCl$ gave brown-black crystals of the product in 89% yield. All details of the synthesis, purification, and characterization of the product by IR (KBr pellet; 400−1000 cm^{-1}), ^{29}Si NMR, and UV−vis spectroscopies, magnetic susceptibility, and elemental analysis (C, H, N, Si, Ru, and W) are given in the Supporting Information. All spectral and analytical data are consistent with this formulation.

III. Results and Discussion

In section III.A we present and discuss the lower lying spin states and geometries of the γ-Ru_2-Keggin polytungstates γ-$[(X^{n+}O_4)Ru_2(OH)_2W_{10}O_{32}]^{(8-n)-}$ for different heteroatoms, X = Al^{III}, Si^{IV}, P^V, and S^{VI}. In section III.B, we extend our studies to the analogous polymolybdates γ-$[(X^{n+}O_4)Ru_2(OH)_2Mo_{10}O_{32}]^{(8-n)-}$ for the same heteroatoms to elucidate the role of frame atoms M_{FM}. In section III.C, we address the synthesis and characterization of $[(n\text{-}C_4H_9)_4N]_4\gamma$-$[(SiO_4)Ru_2(OH)_2(OH_2)_2W_{10}O_{32}]\cdot 2H_2O$.

A. γ-$[(X^{n+}O_4)Ru_2(OH)_2W_{10}O_{32}]^{(8-n)-}$, for X = Al^{III}, Si^{IV}, P^V, and S^{VI}. Let us address the calculated results for the polytungstate γ-$[(X^{n+}O_4)Ru_2(OH)_2W_{10}O_{32}]^{(8-n)-}$, for X = Al^{III}, Si^{IV}, P^V, and S^{VI}. As mentioned above, the geometries of these compounds at their lowest singlet, triplet, and septet spin states were optimized without any geometry constraint, using the B3LYP density functional method with Lanl2dz + d(X) basis sets.[8] Since all calculations converged to C_{2v} (or nearly C_{2V}) structures, in Table 1 we present the important calculated bond distances and relative energies of the $^1A_1$, $^3B_1$, and $^7B_1$ states of these compounds in C_{2v} symmetry.[10,11] The full geometries of these species are given in the Supporting Information. Figure

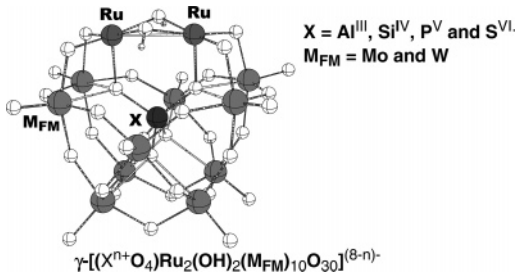

Figure 1. Schematic representation of γ-$[(X^{n+}O_4)Ru_2(OH)_2(M_{FM})_{10}O_{32}]^{(8-n)-}$with X = Al^{III},Si^{IV}, P^V, and S^{VI}.

1 includes a schematic representation of γ-$[(X^{n+}O_4)Ru_2(OH)_2M_{10}O_{32}]^{(8-n)-}$.

As seen in Table 1, the ground electronic state of γ-$[(X^nO_4)Ru_2(OH)_2W_{10}O_{32}]^{(8-n)-}$ varies depending on the central heteroatom, X. For X = Al, the ground state is either the closed shell singlet $^1A_1$ or the triplet $^3B_1$, which are too close to judge from the present level of calculation. On the other hand, for X = S, the high-spin septet state $^7B_1$ is by far the most stable and is the ground state. For the other heteroatoms, a smooth trend holds; for X = Si, all three spin states are similar in energy, and for X = P the ground state is the high-spin septet state $^7B_1$, although this state is not as dominant as in X = S.

The above findings indicate that the heteroatom X largely controls the spin state and electronic structure of this family of γ-Keggin POMs, $[(X^{n+}O_4)Ru_2(OH)_2W_{10}O_{32}]^{(8-n)-}$. Since different spin states usually have very different reactivities, the data suggest that the reactivity of di-d-electron transition-metal-substituted γ-Keggin POMs is partially influenced by the central heteroatom X (which will be addressed in a future study).

As seen in Table 1, the reported systematic change of the electronic state based on X seems to correlate closely with the structural differences between the complexes. In particular, the $X-O_X{}^1$ distance (averaged over different spin states) decreases as X = Al (1.78 Å) > Si (1.65 Å) > P (1.58 Å) > S (1.54 Å). One can relate this trend to the X−O bond strength as well as the size of the X atom. In total asynchrony with this trend, the $Ru-O_X{}^1$ distance for $^1A_1$ ($^7B_1$) states increases from 2.05 (2.36) Å for X = Al, 2.07 (2.45) Å for X = Si, 2.09 (2.56) Å for X = P, and 2.11 (2.93) Å for X = S, with the increase much more drastic for the $^7B_1$ state. These changes occur without significantly changing the size of the entire Keggin "cage". Although this cage is apparently fairly rigid, the $X-O_X$ bond distance changes markedly with the size of X. This is consistent with X-ray crystallographic[12] and computational[13] findings on the plenary Keggin structures (formula: $[X^{n+}W_{12}O_{40}]^{(8-n)-}$). As the $X-O_X$ distance decreases going from X = Al, Si, P to S, the $Ru-O_X$ distance increases, the ligand effect of O_X on Ru becomes weaker, and the Ru atom tends to prefer higher spin states.

The important changes in the bond distances of different electronic states are justified by detailed analysis of frontier orbitals and atomic spin densities. For all four complexes, the $^1A_1$ state HOMO is a Ru−Ru bonding orbital involving Ru $d_{x^2-y^2}$ atomic orbitals with some contributions from the $Ru-O_W$ interactions, while the LUMO is the corresponding Ru−Ru antibonding orbital. The HOMO-1 and HOMO-2 are mainly $Ru^1-O_X{}^1$ and $Ru^2-O_X{}^2$ bonding orbitals with small contributions from the $Ru-O_W$ and $X-O_X$ bonding orbitals; the LUMO+1 and LUMO+2 are the corresponding antibonding orbitals. Therefore, one may expect that the $^1A_1 \rightarrow {}^3B_1$ transition in these compounds corresponds to the Ru−Ru bonding → Ru−Ru antibonding promotion, while the $^3B_1 \rightarrow {}^7B_1$ promotion is associated with the transfer of electrons from HOMO-1 and HOMO-2 orbitals to corresponding LUMO+1 and LUMO+2

TABLE 2: The Calculated Spin Densities (*e*) and $\langle S^2 \rangle$ Values for C_{2v} Optimized Structures of γ-$[(X^{n+}O_4)$-$Ru_2(OH)_2W_{10}O_{32}]^{(8-n)-}$ for X = Al^{III}, Si^{IV}, P^V, and S^{VI}

	X = Al^{III}		X = Si^{IV}		X = P^V		X = S^{VI}	
	$^3B_1$	$^7B_1$	$^3B_1$	$^7B_1$	$^3B_1$	$^7B_1$	$^3B_1$	$^7B_1$
Ru^1	0.91	2.47	0.81	2.49	0.79	2.50	0.76	2.37
$O_b{}^1$	0.02	0.04	0.02	0.04	0.01	0.05	0.03	0.10
$O_X{}^1$	−0.02	0.15	−0.02	0.09	−0.01	0.04	−0.01	0.00
$O_X{}^3$	0.00	0.00	0.00	0.00	0.00	0.00	0.00	0.00
$O_W{}^1$	0.08	0.16	0.08	0.17	0.09	0.18	0.10	0.22
O^1	0.04	0.04	0.04	0.04	0.05	0.04	0.05	0.06
O^2	0.04	0.04	0.04	0.04	0.05	0.04	0.05	0.06
W^1	0.00	−0.02	0.00	0.00	0.00	−0.02	−0.01	−0.02
W^7	0.00	0.00	0.00	0.00	0.00	0.00	0.00	0.00
XO_4	−0.02	0.34	−0.01	0.19	−0.01	0.19	0.00	0.02
$\langle S^2 \rangle$	2.03	12.02	2.03	12.02	2.03	12.02	2.02	12.03

orbitals. This conclusion is consistent with the calculated spin distribution (see Table 2), as well as the changes in geometry parameters. Indeed, as seen in Table 1, the $^1A_1 \rightarrow {}^3B_1$ promotion causes an elongation of the Ru−Ru bond length by 0.444 (X = Al), 0.429 (X = Si), 0.424 (X = P), and 0.417 (X = S) Å, but does not significantly change other geometry parameters. The spin distributions in the $^3B_1$ states are almost the same for all these species; the two unpaired spins are located almost exclusively on the two $(O_W)_2Ru$ units (0.98e each). The energy difference between the singlet and triplet states, $\Delta E(^3B_1 - {}^1A_1)$, is calculated to be only 1.6, 2.7, 1.1, and −2.2 kcal/mol, for X = Al, Si, P, and S, respectively. The similarity of these numbers indicates the involvement of the same orbitals for all species.

The $^3B_1 \rightarrow {}^7B_1$ promotion involves a two-electron promotion from bonding HOMO-1 and HOMO-2 and corresponding antibonding LUMO+1 and LUMO+2. Therefore, it is expected that this promotion results in a significant elongation [0.303 (X = Al), 0.361 (X = Si), 0.457 (X = P), and 0.750 (X = S) Å] of the $Ru^1-O_X{}^1$ and $Ru^2-O_X{}^2$ bond distances, but a slight shortening of the $X-O_X$ bond distances [(0.026 (X = Al), 0.026 (X = Si), 0.026 (X = P), and 0.036 (X = S) Å] and the Ru−O_W bond distances [0.039 (X = Al), 0.040 (X = Si), 0.041 (X = P), and 0.055 (X = S) Å]. These geometry changes are consistent with the calculated spin densities for the $^7B_1$ state; the unpaired spins [2.47e (X = Al), 2.49e (X = Si), 2.50e (X = P), and 2.37e (X = S)] are mainly located on each Ru center, while small fractions are delocalized on each O_X center [0.15e (X = Al), 0.09e (X = Si), 0.04e (X = P), and 0.0e (X = S)] and on each O_W bound to Ru center [0.16e (X = Al), 0.17e (X = Si), 0.18e (X = P), and 0.22e (X = S)], respectively.

As seen in Table 1, the $^3B_1 \rightarrow {}^7B_1$ promotion causes weakening (or cleavage) of $Ru-O_X$ bonds, strengthening of the $X-O_X$ bonds, and a contraction of the central $(X^{n+}O_4)$ unit. As a result, the coordination of the $(X^{n+}O_4)$ unit to the Ru centers is weakened. This stabilizes the high-spin $^7B_1$ state. As discussed above, the stabilization of the $^7B_1$ state relative to the singlet $^1A_1$ state is the calculated $\Delta E(^7B_1 - {}^1A_1)$ energy gap which decreases in the following order: 10.9 (X = Al) > 1.8 (X = Si) > −10.9 (X = P) > −36.1 (X = S) kcal/mol, i.e., the $^7B_1$ state becomes a ground state for the compounds X = P and S.

Thus, aforementioned energies and geometries of several low-lying electronic states of the di-Ru-substituted γ-Keggin POMs, $[(X^{n+}O_4)Ru_2(OH)_2W_{10}O_{32}]^{(8-n)-}$, for X = Al^{III}, Si^{IV}, P^V, and S^{VI}, clearly show that the nature of the heteroatom X in this catalytically significant family of POMs is crucial in defining the lower lying electronic states of the system, which, in its turn, likely impacts reactivity significantly. For the electropositive X = Al^{III}, the ground state is $^1A_1$, while for the more electronegative X = S^{VI} the ground state is the high-spin $^7B_1$ state. Thus, the heteroatom X can be an "internal switch" for determining the ground electronic states and, consequently, the reactivity of the γ-M_2-Keggin POMs. For purposes of experimental verification the computationally predicted γ-$[(SiO_4)Ru_2(OH)_2(OH_2)_2W_{10}O_{32}]^{4-}$ has been prepared and characterized (see Section III.C).

B. γ-$[(X^{n+}O_4)Ru_2(OH)_2Mo_{10}O_{32}]^{(8-n)-}$, for X = Al^{III}, Si^{IV}, P^V, and S^{VI}. To elucidate the role of the "framework atoms", M_{FM}, and validate the aforementioned conclusions for the W-based Keggin structures, we also explored the polymolybdates, γ-$[(X^{n+}O_4)Ru_2(OH)_2Mo_{10}O_{32}]^{(8-n)-}$, for the same X = Al^{III}, Si^{IV}, P^V, and S^{VI}. The results presented in Table 3 clearly show that the conclusions and the trends for polytungstates are valid for their analogous polymolybdate. However, the calculated trends are less pronounced for M_{FM} = Mo than W in the case of X = P and S, which could be explained by the slightly smaller size of the Keggin "cage" in the polymolybdates compared to that of the polytungstates.

Indeed, as seen in Table 3, the $^1A_1 \rightarrow {}^3B_1$ promotion, which corresponds to Ru−Ru bonding → Ru−Ru antibonding promotion, causes weakening (or cleavage) of Ru−Ru bonds. The calculated Ru−Ru elongation, 0.09−0.12 Å, is very close for all investigated polymolybdates, as was the case for the polytungstates. However, this value is somewhat smaller than the 0.40−0.42 Å obtained for the polytungstates. Meanwhile, the $^3B_1 \rightarrow {}^7B_1$ promotion associated with promotion of an electron from a $Ru-O_X$ bonding orbital to the $Ru-O_X$ antibonding orbital leads to the strengthening of the $X-O_X$ bonds, which results in a contraction of the central $(X^{n+}O_4)$ unit. The coordination of the $(X^{n+}O_4)$ unit causes the weakening of the $Ru-O_X{}^1$. In total, as a result of $^3B_1 \rightarrow {}^7B_1$ promotion the $Ru-O_X{}^1$ distance increases from 2.04 to 2.25 Å for X = Al, from 2.05 to 2.32 Å for X = Si, from 2.07 to 2.43 Å for X = P, and from 2.09 to 2.79 Å for X = S. As can be seen from the above-presented discussion and from Table 1, these changes are significantly smaller than analogous changes for the polytung-

TABLE 3: Important Calculated Bond Distances (in Å) and Relative Energies (in kcal/mol) of Low-Lying Electronic States of the γ-$[(X^nO_4)Ru_2(OH)_2Mo_{10}O_{32}]^{(8-n)-}$ for X = Al^{III}, Si^{IV}, P^V, and S^{VI} in C_{2v} Symmetry

	X = Al^{III}			X = Si^{IV}			X = P^V			X = S^{VI}		
bonds	$^1A_1$	$^3B_1$	$^7B_1$	$^1A_1$	$^3B_1$	$^7B_1$	$^1A_1$	$^3B_1$	$^7B_1$	$^1A_1$	$^3B_1$	$^7B_1$
Ru−Ru	2.622	2.716	2.714	2.603	2.701	2.700	2.603	2.721	2.703	2.606	2.704	2.716
$Ru^1-O_b{}^1$	2.085	2.110	2.112	2.079	2.101	2.104	2.076	2.095	2.096	2.073	2.084	2.084
$Ru^1-O_X{}^1$	2.035	2.016	2.253	2.051	2.038	2.318	2.065	2.062	2.430	2.086	2.110	2.787
$Ru^1-O_W{}^1$	1.992	2.000	1.979	1.984	1.986	1.964	1.980	1.979	1.951	1.978	1.973	1.930
$X-O_X{}^1$	1.790	1.794	1.775	1.659	1.662	1.644	1.586	1.588	1.568	1.542	1.535	1.506
$X-O_X{}^3$	1.752	1.749	1.760	1.619	1.617	1.634	1.542	1.542	1.562	1.492	1.503	1.521
$Mo^1-O_W{}^1$	1.894	1.890	1.920	1.886	1.884	1.913	1.886	1.885	1.915	1.890	1.890	1.930
$Mo^1-O_X{}^1$	2.404	2.427	2.345	2.511	2.530	2.441	2.582	2.598	2.499	2.633	2.477	2.505
$Mo^5-O_X{}^3$	2.275	2.274	2.276	2.376	2.371	2.391	2.451	2.441	2.477	2.519	2.477	2.576
$Mo^7-O_W{}^7$	1.947	1.947	1.929	1.939	1.939	1.942	1.936	1.935	1.939	1.935	1.930	1.943
ΔE	0.0	13.0	25.6	0.0	15.3	18.0	0.0	11.6	7.3	0.0	3.1	−11.1

states. As was the case with the polytungstates, the calculated changes in $Ru-O_X$[1] distance for polymolybdates occur without significantly changing the size of the entire Keggin "cage". Again, while the $X-O_X$ bond distance markedly decreases via X = Al > Si > P > S, the $Ru-O_X$ distance decreases via X = Al (0.21 Å) < Si (0.27 Å) < P (0.36 Å) < S (0.70 Å) with the result that the size of the overall Keggin cage is fairly constant. These trends and the overall constancy of the cage (or cluster) size are consistent with many previous structural studies on Keggin polyoxometalates.[12] These geometry changes stabilize the high-spin $^7B_1$ state of the systems relative to the low-spin state $^1A_1$. As seen in Table 3, the calculated $\Delta E(^7B_1-{}^1A_1)$ energy gap decreases in the order 25.6 (X = Al) > 18.0 (X = Si) > 7.3 (X = P) > −11.1 (X = S) kcal/mol. The same trend is reported above for the investigated polytungstates: 10.9 (X = Al) > 1.8 (X = Si) > −10.9 (X = P) > −36.1 (X = S) kcal/mol. Comparison of these values of $\Delta E(^7B_1-{}^1A_1)$ for polytungstates and polytungstates clearly shows that stabilization of the high-spin states of γ-M_2-Keggin POMs upon changing of heteroatom X via $Al^{III} > Si^{IV} > P^V > S^{VI}$ is more pronounced for the polytungstates than for the polymolybdates. Therefore, one may expected that the γ-M_2-Keggin polytungstates are more reactive than their polymolybdate analogues.

C. Synthesis and Characterization of the γ-$[(SiO_4)Ru^{III}{}_2(OH)_2(OH_2)_2W_{10}O_{32}]^{4-}$. To provide additional experimental background for the computational studies reported here, a representative γ-Ru_2-Keggin POM, namely γ-$[(SiO_4)Ru_2(OH)_2(OH_2)_2W_{10}O_{32}]^{4-}$, was targeted. This complex was successfully synthesized, purified ,and characterized by ^{29}Si NMR, FT infrared, optical spectroscopies, magnetic susceptibility, and elemental analysis. All data (given in the Supporting Information) are consistent with the proposed complex. Indeed, elemental analysis shows that the prepared complex can be formulated as $[(n\text{-}C_4H_9)_4N]_4[\gamma\text{-}SiW_{10}Ru_2(OH)_2(H_2O)_2O_{36}]\cdot 2H_2O$. ^{29}Si NMR (79.456 MHz, 3.6 MTMS in $CDCl_3$ standard) revealed a very broad peak with an approximate chemical shift of −85 ppm. UV−vis in CH_3CN revealed one sharp band at 462 nm (1.2×10^4 $M^{-1}\cdot cm^{-1}$) attributed to d−d ligand field transitions and a shoulder at 600 nm (0.32×10^4 $M^{-1}\cdot cm^{-1}$). The poorly resolved shoulders at 273 (3.3×10^4 $M^{-1}\cdot cm^{-1}$) and 330 nm (1.2×10^4) are indicative of the γ-Keggin anion. The room-temperature magnetic moment calculated from the magnetic susceptibility analysis is 1.4 μ_B.

IV. Concluding Remarks

The computational results presented above for the di-Ru-substituted γ-Keggin POMs, $[(X^nO_4)Ru_2(OH)_2(M_{FW})_{10}O_{32}]^{(8-n)-}$ for M_{FM} = Mo and W, and X = Al^{III}, Si^{IV}, P^V, and S^{VI}, clearly show that the nature of the heteroatom X in this catalytically significant family of POMs is crucial in determining the lower lying electronic states of the system. These states, in turn, likely impact reactivity to a good extent. For M_{FM} = W, with the electropositive heteroatom X = Al^{III}, the ground state is $^1A_1$, while for the more electronegative heteroatom X = S^{VI}, the ground state is the high-spin $^7B_1$. In other words, the heteroatom X can function as an "internal switch" for controlling the ground electronic states and, consequently, the reactivity of this family of disubstituted catalytically significant polytungstates.

The same trends in energies and geometries were found for the analogous polymolybdates, $[(X^nO_4)Ru_2(OH)_2(Mo)_{10}O_{32}]^{(8-n)-}$ for X = Al^{III}, Si^{IV}, P^V, and S^{VI}. However, the obtained trends, in general, are less pronounced for M_{FM} = Mo than W. On the basis of the comparison of the calculated energy gaps between low-spin and high-spin states of polytungstates and polymolybdates, it is predicted that the γ-M_2-Keggin polytungstates could be more reactive than their polymolybdate analogues.

For purposes of experimental verification, the computationally predicted γ-$[(SiO_4)Ru_2(OH)_2(OH_2)_2W_{10}O_{32}]^{4-}$ was prepared and thoroughly characterized.

Acknowledgment. The present research is supported by a grant (DE-FG02-03ER15461) from the Department of Energy. Computer resources were provided in part by the Air Force Office of Scientific Research DURIP grant (FA9550-04-1-0321), as well as by the Cherry Emerson Center for Scientific Computation at Emory University, and by the DOE PNNL EMSL facility under the GC3568 grant.

Supporting Information Available: Synthesis, spectroscopic properties, and elemental analyses of γ-$[(SiO_4)Ru_2(OH)_2(OH_2)_2W_{10}O_{32}]^{4-}$; Optimized Cartesian coordinates of all structures; and completed ref 9. This material is available free of charge via the Internet at http://pubs.acs.org.

References and Notes

(1) Recent reviews of POMs: (a) Topical issue on polyoxometalates: Hill, C. L. Guest Ed. *Chem. Rev.* **1998**, *98*, 1. (b) *Polyoxometalate Chemistry*: *From Topology via Self-Assembly to Applications*; Pope, M. T., Müller, A., Eds.; Kluwer: Dordrecht, The Netherlands, 2001. (c) *Polyoxometalate Chemistry for Nano-Composite Design*; Yamase, T., Pope, M. T., Eds.; Kluwer: Dordrecht, The Netherlands, 2002. (d) Hill, C. L. Polyoxometalates: reactivity. In *Comprehensive Coordination Chemistry II*: *Transition Metal Groups 3*−*6*; Wedd, A. G., Ed.; Elsevier Science: New York, 2004; Vol. 4, Chapter 4.10, pp 679−759.

(2) Pope, M. T. Polyoxo Anions: Synthesis and Structure. In *Comprehensive Coordination Chemistry II*: *Transition Metal Groups 3*−*6*; Wedd, A. G., Ed.; Elsevier Science: New York, 2004; Vol. 4, Chapter 4.09, pp 635−678.

(3) Structurally characterized γ-M_2-Keggin complexes: (a) Wassermann, K.; H.-J.; Lunk, H. -J.; Palm, R.; Fuchs, J.; Steinfeldt, N.; Stösser, R.; Pope, M. T. *Inorg. Chem.* **1996**, *35*, 3273−3279. (b) Zhang, X.-Y.; O'Connor, C. J.; Jameson, G. B.; Pope, M. T. *Inorg. Chem.* 1**996**, *35*, 30−34. (c) Cadot, E.; Béreau, V.; Marg, B.; Halut, S.; Sécheresse, F. *Inorg. Chem.* **1996**, *35*, 3099−3106. (d) Xin, F.; Pope, M. T. *Inorg. Chem.* **1996**, *35*, 5693−5695.

(4) (a) Nishiyama, Y.; Nakagawa, Y.; Mizuno, N. *Angew. Chem., Int. Ed.* **2001**, *40*, 3639−3541. (b) Kozhevnikov, I. V. *Catalysis by Polyoxometalates*; Wiley & Sons: Chichester, England, 2002.

(5) (a) Becke, A. D. *Phys. Rev. A* **1988**, *38*, 3098−3107, (b) Becke, A. D. *J. Chem. Soc.* **1993**, *98*, 1372−1380.

(6) Lee, C.; Yang, W.; Parr, R. G. *Phys. Rev. B* **1988**, *37*, 785−789.

(7) (a) Hay, P. J.; Wadt, W. R. *J. Chem. Phys.* **1985**, *82*, 299−310. (b) Hay, P. J.; Wadt, W. R. *J. Chem. Phys.* **1985**, *82*, 270−283. (c) Wadt, W. R.; Hay, P. J. *J. Chem. Phys.* **1985**, *82*, 284−298.

(8) Musaev, D. G.; Morokuma, K.; Geletii, Y. V.; Hill C. L. *Inorg. Chem.* **2004**, *43*, 7702−7708.

(9) Frisch, M. J. T.; et al.; *Gaussian 2003*; Gaussian, Inc.: Pittsburgh, PA, 2003.

(10) Analyses show that the lowest quintet states of these compounds cannot be properly described with the single-determinant approaches such as B3LYP used in this paper. Therefore, the quintet states of these species will not be discussed in this paper. Significantly, they have no affect on our final conclusions.

(11) It is well established (see: Quiñonero, D.; Musaev, D. G.; Morokuma, K. *Inorg. Chem.* **2003**, *42*, 8449−8457) that hybrid density functional approaches (such as B3LYP) overestimate the stability of high-spin states relative to low-spin states. Therefore, we have performed optimization geometry and energy calculations for compound $[(SO_4)Ru_2(OH)_2W_{10}O_{32}]^{2-}$ using the nonhybrid BLYP functional. It was found that the use of the BLYP method does not change the conclusions of this paper, while it reduces the calculated $\Delta E(^7B_1-{}^1A_1)$ energy gap from 36.1 kcal/mol to 24.4 kcal/mol.

(12) Neiwert, W. A.; Cowan, J. J.; Hardcastle, K. I.; Hill, C. L.; Weinstock, I. A. *Inorg. Chem.* **2002**, *41*, 6950−6952 and references therein.

(13) Lopez, X.; Maestre, J. M.; Bo, C.; Poblet, J.-M. *J. Am. Chem. Soc.* **2001**, *123*, 9571−9576.